Performance-based optimization of steel exoskeletons: An alternative approach to standard regulations

Journal of Building Engineering 104 (2025) 112177

Contents lists available at ScienceDirect

Journal of Building Engineering

journal homepage: www.elsevier.com/locate/jobe

Full length article

Performance-based optimization of steel exoskeletons: An alternative approach to standard regulations

Raffaele Cucuzza [a,b], Jana Olivo [b,*], Gabriele Bertagnoli [b], Giuseppe Andrea Ferro [b], Giuseppe Carlo Marano [b]

[a] College of Civil Engineering, Henan University of Technology, Zhengzhou, Henan Province, China
[b] Politecnico di Torino, Department of Structural, Geotechnical and Building Engineering, Corso Duca Degli Abruzzi, 24, Turin, 10128, Italy

ARTICLE INFO

Keywords:
Exoskeletons
Performance-based design
Inter-story drift
Earthquake
Genetic algorithm

ABSTRACT

Among the various seismic retrofitting techniques, steel exoskeletons are distinguished as a valuable retrofitting approach to mitigate structural vulnerability under lateral loads while simultaneously preserving the buildings' functionality and activities' full operability. However, they are not a commonly selected option by designers, as several standard regulations recommend a design approach based on the relative stiffness between the exoskeletons and the building. They establish a restrictive limit for this ratio, resulting in costly and heavy designs. This paper proposes a paradigm shift in exoskeleton design, moving from the control of the stiffness ratio to a performance-based design approach. Different inter-story drift thresholds are adopted as performance constraints of an innovative optimized design procedure where the number, position, and sizing of the exoskeletons are assumed as design variables. Based on the outcomes of the optimization processes conducted on three real-world inspired case studies, a sensitivity analysis is performed. In all scenarios, the results demonstrate that the performance-based approach allows for greater utilization of the building's capacity in the elastic field to resist horizontal actions while preserving structural safety. Consequently, in contrast with the conservative designs obtained following standard regulations, the proposed approach leads to lighter and more economically efficient designs, which make the exoskeletons a more attractive alternative.

1. Introduction

Several countries, especially in Europe, count many buildings that were constructed prior to the introduction of the current seismic regulations [1,2]. Additionally, most of them have exceeded their design life spans, presenting safety and durability issues [3,4].

In this context, there is a pressing need for large-scale renovation plans, but the traditional retrofitting approaches fail to overcome some challenges [5–7]. One of the main issues is related to the relocation of the inhabitants in residential buildings, or the interruption of the activities carried out within strategical structures [8,9]. Moreover, the implementation of such interventions often represents considerable economic costs, in addition to the technical challenges that may rise due to the lack of viable alternatives to address the specific case requirements [10].

In recent decades, steel exoskeletons have gained significant attention as a means of overcoming most of the aforementioned challenges [11]. These systems are applied from the exterior of the building, being non-invasive and time-efficient [12,13].

* Corresponding author.
E-mail address: jana.olivo@polito.it (J. Olivo).

https://doi.org/10.1016/j.jobe.2025.112177
Received 30 October 2024; Received in revised form 9 February 2025; Accepted 18 February 2025
Available online 5 March 2025

Exoskeletons retrofit the building by increasing its stiffness and resistance to horizontal forces, thereby significantly unloading the existing structure [14]. These structures can be either two-dimensional or three-dimensional [15] as well as connected perpendicularly [16,17] or parallelly [18,19] to the facade of the existing building. Additionally, they can enhance the structural performance of the building either by increasing the system's stiffness or by accommodating dissipative devices [20–22].

It is noteworthy that, in a context in which sustainability aspects in the construction sector have received great attention from the scientific and professional community [23–26], this solution has the potential to align with the Life Cycle Thinking principles [27,28]. Furthermore, as demonstrated by several real-world application case studies [29,30], the design of a holistic intervention with exoskeletons is often practicable [31,32], addressing the structural safety [33] while simultaneously enhancing the energetic performance [34,35], and aesthetic value [36–38] through the creation of a second façade of the building [39,40].

Even if steel exoskeletons represent a promising solution, limited consolidated methodologies for their design have been proposed so far [41,42]. Existing studies on the subject propose the determination of the overall stiffness and mass of the exoskeletons [43,44]. This is usually accomplished through the simplification of the building-exoskeleton assembly as two coupled Single-Degree-of-Freedom systems [45]. Nevertheless, these approaches do not address crucial aspects of the design, such as the distribution of the exoskeletons or the sizing of their components [17,46] while connection details are provided just for specific engineering application case studies [47].

Despite this, several standard regulations, such as the NTC 18 [48], the Eurocode 8 [49], and the ASCE 41-17 [50], propose a design criterion based on a classification of the elements of the structure into primary and secondary according to their stiffness. This classification can be useful for retrofitting approaches through exoskeletons and is generally employed by several practitioners. Following this approach, designers are usually constrained to comply with a minimum stiffness performance to be assigned to exoskeletons (i.e., primary element) with the advantage of neglecting structural verification of the elements of the existing building (secondary element). Practically, this distinction can be adopted for an acceptable threshold value expressed as a ratio between the stiffness of the exoskeletons and the stiffness of the existing building. As demonstrated by the authors, the disadvantage is that this approach leads to almost completely unloading the existing building, underestimating its capacity to resist horizontal actions. As a consequence, the obtained configurations are generally oversized and imply high costs.

Aiming to address the aforementioned issues, the present work proposes a paradigm shift in the design of exoskeletons, moving from stiffness ratio control (approach currently adopted by Standard codes) to a performance-based design approach. The main design parameter is the inter-story drift (ISD) [51–53], and a sensitivity analysis was conducted to evaluate the influence of the ISD threshold on the structural behavior of the system. For each threshold, an optimization process was conducted [54], through which the final configuration was defined in terms of the number and spatial placement of the exoskeletons, as well as the dimensions of their constituent elements. These three aspects of the design constitute the *Design Variables (DVs)* of the optimization problem while the *Objective Function (OF)* is expressed in terms of structural cost (i.e. weight) [55]. Moreover, the optimal solution must ensure compliance with two *constraints*: the inter-story drift threshold and the structural verifications of the exoskeleton elements. The versatility and applicability of the developed intelligent design procedure in diverse building environments are preserved by the strong adaptability of the design parameters. These parameters can accommodate variations in structural typologies and geometries of the existing building, surrounding conditions related to the presence of adjacent structures, and architectural constraints. The algorithm could be easily customized to satisfy specific geometric constraints according to case-by-case design challenges.

Three different reinforced concrete (RC) buildings are analyzed in this study, encompassing a range of complexities and in-plan irregularities. The buildings were selected to provide a representative sample of a significant portion of the European built environment. Furthermore, Finite Element analyses and structural verifications are performed through the SAP2000 Open Application Programming Interface (OAPI) accounting for the dynamic change of the exoskeleton design along the entire iterative procedure. The modeling strategies as well as the level of precision of the investigated three-dimensional models ensure an accurate assessment of the seismic behavior overcoming the design simplification observed in the literature.

The results demonstrate the effectiveness of steel exoskeletons as a retrofitting solution for resisting horizontal actions. The efficacy of this retrofitting technique was analyzed in terms of (i) safety level according to European regulation, (ii) the unloading ratios of the building, and (iii) the inter-story drift control assumed as the dominant performance parameter for the design of exoskeletons. The conducted sensitivity analyses led to a better understanding of the dependencies between different inter-story drift thresholds and the structural safety of the buildings retrofitted with different exoskeletons' designs. Additionally, the ratios between the horizontal stiffness of the exoskeletons and that of the building were determined for each of the obtained optimal configurations. Finally, a comparison between the stiffness ratios calculated by the authors and those specified in the standard regulations was presented, demonstrating that a significant reduction in the structural weight of the exoskeletons can be attained through this methodology.

This paper is organized as follows: in Section 2, the approach proposed by some standard regulations is summarized and discussed, and an alternative approach is proposed. In Section 3, the methodology is presented, encompassing the details of the proposed performance-based approach and the optimization tool. In Section 4, the case studies are introduced, presenting the considered buildings and the exoskeleton layout. In Section 5, the optimal configurations of exoskeletons are analyzed, and the characteristics of the results obtained with the displacement-based approach are compared with the code provisions. In Section 6, the simplified approach used to consider non-linear effects is described and its results are presented. In Section 7 the safety level associated with different inter-story drift thresholds is analyzed. Finally, the conclusions of the work and future developments are presented in Section 8.

Table 1
Primary and secondary elements definition according to NTC18 [48], Eurocode 8 [49] and ASCE 41-17 [50]. λ factor accounts for the percentage of horizontal action taken from secondary elements.

Italy NTC 18	Eurocode 8	ASCE 41-17
Secondary elements definition		
Some structural elements can be considered "secondary"; in the analysis of seismic response, the stiffness and resistance to the horizontal actions of these elements can be neglected.	Secondary seismic members are members which are not considered as part of the seismic action resisting system and whose strength and stiffness against seismic actions is neglected.	A secondary component is an element that accommodates seismic deformations but is not required to resist the seismic forces it may attract for the structure to achieve the selected Performance Level.
Unloading ratio definition and λ factor		
In no case the total contribution to stiffness and strength under horizontal actions of secondary elements can exceed the **15%** of the analog contribution of the primary elements.	The total contribution to lateral stiffness of all secondary seismic members should not exceed **15%** of that of all primary members.	If the total initial lateral stiffness of secondary components in a building exceeds **25%** of the total initial lateral stiffness of primary components, some secondary components shall be reclassified as primary.
Design criteria and requested verifications		
The secondary elements and their connections must therefore be designed and equipped with constructive details to withstand the gravitational loads, when subjected to displacements caused by the most unfavorable of the design seismic conditions of the Collapse Limit State.	These members and their connections shall be designed and detailed to maintain support of gravity loading when subjected to the displacements caused by the most unfavorable seismic design condition. Due allowance of 2nd order effects (P-Δ effects) should be made in the design of these members.	Secondary components shall be evaluated for earthquake-induced deformations in combination with gravity load effects. Mathematical models for use with linear analysis procedures shall include the stiffness and resistance of only the primary components.

2. Stiffness ratio approach by standard regulations

Several current standards propose the classification of the elements of a structure as primary or secondary. For this review, the Italian standard NTC18 [48], the European standard Eurocode 8 [49], and the American standard ASCE 41-17 [50] were analyzed. Key aspects of this approach are identified for each code and reported in Table 1.

In summary, the standards allow for certain structural elements to be considered secondary. Standard codes agree on neglecting resistance requirements of these elements under horizontal actions while structural checks under gravitational forces are still required when subjected to deformations produced by the earthquake (i.e., 2nd order effects).

However, the standards specify the maximum force to which secondary elements can be subjected. It is stated that the total contribution of the secondary elements to the stiffness and resistance to horizontal actions cannot exceed a specified percentage (λ factor in Table 1) of the analogous contribution of the primary elements.

This classification can be pertinent when designing interventions with exoskeletons. Due to the typically low level of knowledge of the original structure and the expected non-ductile behavior of RC structures, neglecting the verification of its elements can yield significant benefits. Additionally, since these elements do not contribute to the resistance to horizontal actions, extensive local interventions can be avoided.

It is important to note that determining whether an element is primary or secondary often requires a significant understanding of the stress distribution within the existing structure, which is generally difficult to achieve. Consequently, when designers adopt this approach, they are frequently constrained to consider the entire existing structure as secondary. In this case, the total horizontal stiffness of the building must not exceed a value of λ of the total horizontal stiffness of the exoskeletons, which represent the primary elements. Therefore, the stiffness value of the exoskeletons, according to the most conservative regulations (Italian NTC18 and European Eurocode 8 Standard Code), can assume at least 6.67 times that of the existing structure, as calculated below:

$$K_{ratio} = \frac{K_{exosk}}{K_{building}} = \frac{100}{15} = 6.67$$

This raises the question of whether the stiffness ratio approach is the sole or most efficient method to ensure structural safety while guaranteeing an optimized design of the retrofitting system. In this paper, the authors introduce an alternative method to the stiffness ratio control parameter where displacement control (i.e. inter-story drift) is adopted to ensure proper structural safety levels while accounting for the economic cost of the retrofitting solution. The integration of such a novel approach into current Standard Codes could undoubtedly enhance the perspective design of retrofitting systems such as exoskeletons and provide valid support to practitioners intending to adopt this type of intervention as a promising solution for real-world civil engineering applications. In this sense, the pressing need to rehabilitate the built environment from an energetic and aesthetic perspective could provide an opportunity to promote eco-friendly and low-CO_2 emission retrofitting solutions, as an alternative to traditional approaches.

3. Methodology

In this section, the philosophy behind the developed performance-based optimization framework for the design of exoskeletons is introduced, wherein inter-story drift (ISD) thresholds are selected as the primary design parameter because of their crucial role in the assessment of seismic forces transferred by the existing building to exoskeletons.

Table 2
Inter-story drift limits (as % of story height H) associated with different performance levels defined by Ghobarah [56] (for ductile (D MRF) and non-ductile (ND MRF) moment resisting frames), Lu et al. [57], and FEMA 356 [58].

Perf. Level	Ghobarah D MRF %H	Ghobarah ND MRF %H	Perf. Level	Lu et al. %H	Perf. Level	FEMA 356 %H
Light Damage	0.4	0.2		–		–
Moderate Damage	<1.0	<0.5	Functional Level	^{m} 1.0	Immediate Occupancy	1.0
Irreparable Damage	>1.0	>0.5	Damage Control	^{m} 2.0–4.5 ^{c} 0.8–2.2	Life Safety	2.0
Collapse	>3.0	>1.0	Ultimate Level	^{m} 3.0–7.8 ^{c} 1.1–3.3	Collapse Prevention	4.0

^{m}: mean value, ^{c}: characteristic value (with 95% probability of being exceeded).

Based on previous studies, Section 3.1 is entirely dedicated to the evaluation of various ISD thresholds for the definition of a suitable performance target range, associated with a specific level of damage, expected by the system. Depending on the assumed ISD threshold, the authors conducted a sensitivity analysis to evaluate the structural and safety response of the system.

Finally, Section 3.2 introduces the formulation of the optimization process as well as provide further detail on the implementation of the performance-based approach within a population-based evolutionary algorithm.

3.1. Performance-based approach

In this paper, the authors introduce an alternative method to the traditional stiffness ratio control, where displacement control (i.e. inter-story drift) is adopted to ensure proper structural safety levels and limit the structural damage, while accounting for the economic cost of the retrofitting solution.

The definition of drift limits associated with different damage levels has been already approached in literature; these values have been reported in Table 2 for the different performance levels. Ghobarah [56] determined the inter-story drift of diverse structural systems associated with different levels of damage, using analytical and experimental data. The limits presented in Table 2 correspond to ductile (D) and non-ductile (ND) Moment Resisting Frames (MRF). Lu et al. [57] determined the probabilistic drift limits of RC columns at three performance levels, using Monte Carlo simulation and a statistical model of the plastic hinge length. The standard FEMA 356 [58] provides typical drift values associated with various structural performance levels for concrete frames. Finally, the Eurocode 8 [49] defines inter-story drift limits as damage limitation requirements. The provided values are 0.5%H in cases where non-structural elements are brittle, 0.75%H where these are ductile, and 1%H in cases without non-structural elements or when these do not interfere with the deformations.

Elastic displacement thresholds associated with *light damage* (see Table 2) will be used for the formulation of the performance-based optimization framework. Six inter-story drift thresholds ($\frac{H_{story}}{\beta}$) are analyzed for each building. H_{story} represents the height of the story, while for β, the different inter-story drift values 400, 450, 500, 550, 600, and 650, have been adopted. These values are selected according to the performance limits defined by Ghobarah [56], where $H_{story}/500$ represents the reference displacement limit equal to $0.2\%H_{story}$ of the vulnerable system associated with light damage on non-ductile MRF. In this way, the effect of a broader range of displacement targets around this reference performance value has been investigated to explore both less and more restrictive limits.

The selected light damage threshold guarantees that the structure works within the elastic field under the seismic action, not reaching the yielding of the reinforcement bars or the ultimate compressive stress in the concrete. Consequently, multimodal dynamic analyses can be identified as a promising and efficient approach for predicting the structural response of the building-exoskeleton systems.

As proof of this, the authors conducted further analysis by validating the obtained optimal configurations through non-linear static (pushover) analyses, to assess the effect of material non-linearities. To account for the effects of concrete cracking, linear dynamic analyses with reduced concrete stiffness of the building were also conducted to validate the analysis typology. This value was reduced to one-fourth of its original value, representing the potential concrete cracking. The results, which are presented in Section 5, demonstrate that the increase in required steel due to the decrease in concrete stiffness is negligible, validating the obtained results.

3.2. Optimization framework

The evolutionary strategy of the Genetic Algorithm (GA) has been adopted for the implementation of the optimization process. The Formulation of the optimization problem as well as the definition of the design variables is inspired by a previous work published by the authors [55]. However, in the following, upgrades and modifications of the existing algorithm are clearly introduced complying with the performance-based design approach proposed in the current work.

The aim of the optimization process is to identify the exoskeletons' configuration and sizing that results in the lowest possible weight while ensuring structural safety. This is guaranteed through the imposition of an inter-story drift threshold, which represents the dominant control parameter accounting for the expected level of damage to the structure, and the structural verification of the exoskeleton elements. The mathematical formulation of the optimization is presented through the definition of the Objective Function (OF) in Eq. (1), the Design Variables (DVs) in Eqs. (2)–(3), the Constraints in Eqs. (4)–(6), and the Penalties in Eqs. (7)–(9).

$$\textbf{min } f = W_{Ex} \cdot \phi_1(D_i) \cdot \phi_2(S_j) + \phi_3(N_{Ex}) \tag{1}$$

$$\mathbf{x} = [\overbrace{x_1, \dots, x_i, \dots, x_n}^{\text{Topology DV}}, \overbrace{x_{n+1}, \dots, x_{n+j}, \dots, x_{n+m}}^{\text{Size DV}}] \tag{2}$$

Subjected to:

$$x_i = \begin{cases} 0 \\ 1 \end{cases} \quad ; \quad x_{n+j}^{lower} < x_{n+j} < x_{n+j}^{upper} \tag{3}$$

$$D_i = \frac{\delta_i}{\delta_{allowable}} < 1 \quad \forall\, i = 1, \dots, N_{nodes} \quad ; \quad \delta_{allowable} = \frac{H_{story}}{\beta} \tag{4}$$

$$S_{j,1} = \frac{N_{Ed}}{\chi_a \cdot N_{Rd}} + \sqrt{\left(k_{ay} \cdot \frac{M_y^{Ed} + N_{Ed} \cdot e_{N_y}}{\chi_{LT} \cdot M_y^{Rd}}\right)^2 + \left(k_{az} \cdot \frac{M_z^{Ed} + N_{Ed} \cdot e_{N_z}}{M_z^{Rd}}\right)^2} < 1 \tag{5}$$

$$S_{j,2} = \frac{V_{Ed}}{V_{pl,T,Rd}} < 1 \quad ; \quad V_{pl,T,Rd} = \left[1 - \frac{\tau_{t,Ed}}{(f_y/\sqrt{3})/\gamma_{M0}}\right] V_{pl,Rd} \tag{6}$$

Penalties:

$$\phi_1 = \sum_{i=1}^{N_{nodes}} D_i^{inf} \tag{7}$$

$$\phi_2 = \sum_{j=1}^{N_{Ex}} \sum_{i=1}^{N_{el}} S_{i,j}^{inf} \quad ; \quad S_{i,j} = max \left\{ S_{i,j,1} \, ; \, S_{i,j,2} \right\} \tag{8}$$

$$\phi_3 = \alpha \cdot N_{Ex} \tag{9}$$

The Objective Function (Eq. (1)) is given by the minimization of the exoskeletons' weight (W_{Ex}), affected by the penalties ϕ_1, ϕ_2, and ϕ_3. The first two penalties are functions of the defined constraints (Eqs. (4)–(6)), while the last penalty is aimed at decreasing the number of exoskeletons (N_{Ex}) in the optimal configuration.

The design variables represent the quantity and spatial arrangement of the exoskeletons, as well as the steel profiles assigned to their constituent elements. These are defined in the vector in Eq. (2), in which two distinct variable typologies are identified. The Topology DVs define the amount and position of the exoskeletons. The amount of Topology DVs is equal to the number of positions where an exoskeleton could be positioned. These variables are binary (Eq. (3)); if the final value of the variable is 1, an exoskeleton is placed in the corresponding position, conversely, if it is 0, the position is left free.

Meanwhile, the Size DVs represent the steel cross-section selected for each element of the exoskeletons. Each exoskeleton is composed of nine steel profiles, derived from a grouping of the elements, as depicted in Fig. 5. All exoskeletons within a configuration are identical; therefore, the Size DVs are 9. The values these can take correspond to a steel profile in a list of 150 different Circular Hollow Sections (CHS), according to the European code EN10219-2.

The first constraint refers to the imposition of the inter-story drift threshold, as defined in Eq. (4). To comply with this constraint, the ratio between the inter-story drift of each node (N_{nodes}) of the reinforced concrete (RC) building (δ_i) and the maximum inter-story drift allowable ($\delta_{allowable}$), called D_i, must be lower than 1. In detail, δ_i is defined as the difference between the displacement of the ith node and the displacement of the corresponding node in the floor directly below it. The threshold, $\delta_{allowable}$, is defined as the ratio between the story height H_{story} and a factor β. Different values of β have been considered for this analysis, ranging from 400 to 650, performing an independent optimization for each $\delta_{allowable}$.

To incorporate this constraint into the OF, the first penalty ϕ_1 is employed. For its definition, the ratio D_i is determined for all the nodes of the structure (N_{nodes}), and the nodes with a corresponding D_i higher than 1 are considered infeasible (D_i^{inf}). Subsequently, as presented in Eq. (7), the sum of all the D_i^{inf} is calculated to obtain the value of ϕ_1. This value then multiplies the weight of the exoskeletons W_{Ex} in the OF (Eq. (1)). In this way, both the quantity and severity of the constraint violations are considered in the OF.

The second constraint represents the structural verifications that the exoskeleton's elements must comply with, according to Eurocode 3 [59]. Then, $S_{j,n}$ are the Demand–Capacity Ratios (DCR) of the jth exoskeleton element according to the n_{th} structural verification. To comply with the constraint, these must be lower than 1. Specifically, $S_{j,1}$ defined in Eq. (5) refers to the combined bending and axial compression, accounting for buckling, according to EC3 6.3.3.(6.61–6.62). Instead, $S_{j,2}$ defined in Eq. (6) refers to combined shear force and torsional moment, as specified in EC3 6.2.7.(6.25) and (6.28). As specified in Eq. (8), the structural

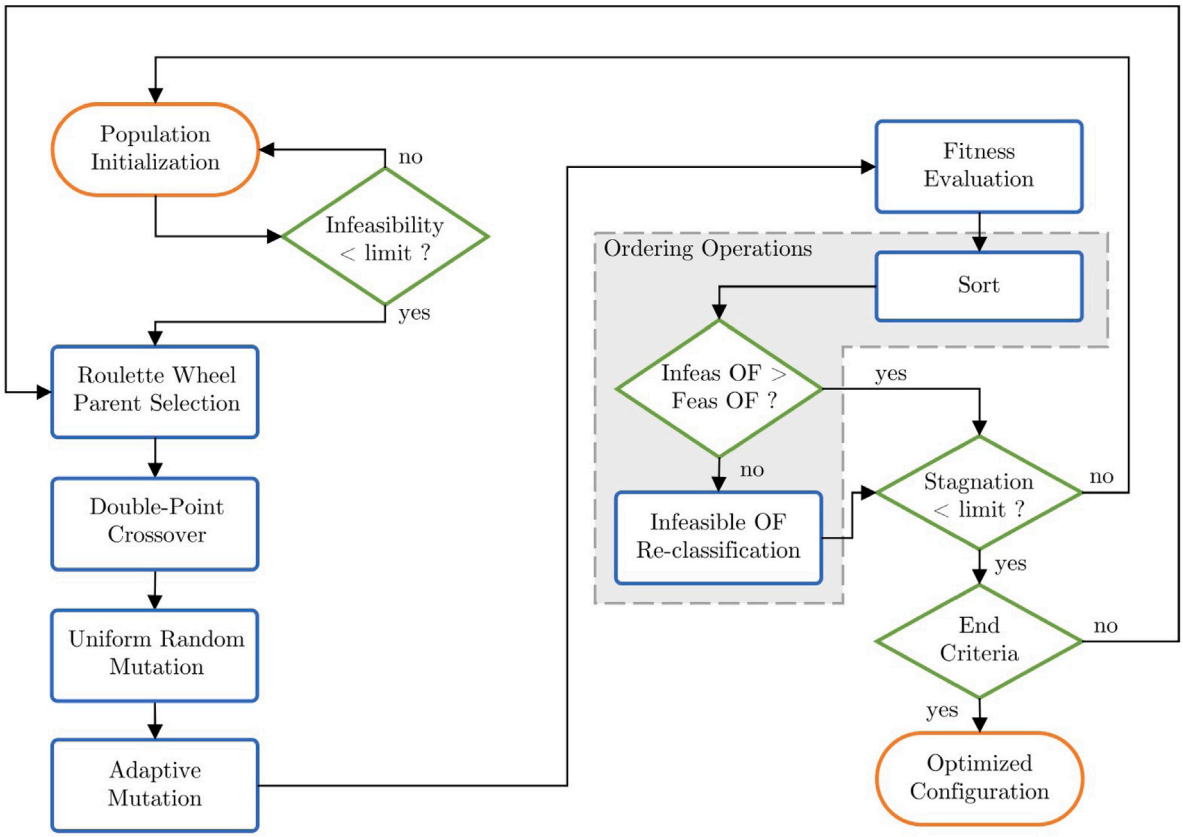

Fig. 1. Flowchart of the adapted Genetic Algorithm employed for the optimization process proposed by Olivo et al. [55].

verifications are conducted for all elements of all exoskeletons, where N_{Ex} is the total number of exoskeletons in the configuration and N_{el} denotes the number of elements per exoskeleton.

In the same way as for ϕ_1, the second penalty ϕ_2 is defined to incorporate the second constraint within the OF. The Demand–Capacity Ratios, $S_{j,n}$, are determined for each of the j exoskeleton's elements. For each element, the DCR considered is the maximum between $S_{j,1}$ and $S_{j,2}$. The values exceeding 1 are considered infeasible and designated as $S_j^i nf$. As was done in the determination of ϕ_1, the infeasible values are summed to obtain the penalty ϕ_2, as presented in Eq. (8). This value then multiplies the weight of the exoskeletons in the OF.

Conversely, the last penalty (ϕ_3) is introduced in order to consider implicitly constructability issues from the construction process. A final configuration with a lower number of exoskeletons is preferable for several reasons. The required free space around the building increases in proportion to the number of exoskeletons, as well as the transportation, assembly, and erection times and costs. Moreover, the RC column-beam nodes to which the exoskeletons are connected typically require local retrofitting interventions, and a reduction in the number of exoskeletons entails a reduction in these interventions. Therefore, ϕ_3 is defined in Eq. (9) as the total number of exoskeletons N_{Ex} by a factor α defined as 10 for this study. This value is added to the exoskeletons' weight already multiplied by ϕ_1 and ϕ_2.

Details about the calibration procedure of the penalty functions, convergence rate of the algorithm, the accuracy and reliability of the optimization procedure are available in [55]. The step-by-step procedure and the main operators of the optimization algorithm are illustrated in the flowchart in Fig. 1.

As detailed in [55], the implemented Genetic Algorithm (GA) employs conventional GA operators for the parent selection, crossover, and mutation. However, case-specific strategies have been developed, including Adaptive Mutation and Ordering Operations, aimed at enhancing the exploitation of the algorithm while avoiding rapid convergence.

For the Fitness Evaluation, each individual's stresses and displacements have been determined by conducting Finite Element Analyses in SAP2000. The creation and modification of the Finite Element Models were executed through automatic routines, governed by the algorithm in MATLAB. Multimodal dynamic analyses were conducted using the response spectrum of Foggia, Italy. The spectrum corresponds to a non-dissipative behavior of the RC building (*behavior factor*, q, equal to 1) complying with the expected elastic response of the building after the intervention.

The eigenvalue and eigenvector problem is solved, and the modal responses, associated with each vibration mode, are combined using the Complete Quadratic Combination (CQC) or the square root of the sum of squares (SRSS) method [49]. Modal analyses

Table 3
Optimization parameters selected for each Case Study (CS#) in terms of quantity of design variables (Topology DVs + Size DVs), population size, and number of iterations; and main characteristics of the unretrofitted buildings in terms of number of critical elements (with DCR > 0.9) over total number of elements, maximum and average Demand–Capacity Ratio (DCR), initial top displacement, and inter-story drift (ISD).

	CS1	CS2	CS3
Variables	16 + 9	20 + 9	34 + 9
Population size	100	150	200
Num. iterations	200	200	200
Seismic mass [ton]	218.5	507.4	906.3
Critical elem./total	93/114 = 82%	149/182 = 82%	337/405 = 83%
Max. DCR	2.15	2.26	2.17
Avg. DCR	1.37	1.31	1.40
Top disp. [mm]	87.2	97.9	83.5
Max. ISD [mm]	37.2	41.5	36.2

automatically consider the number of modes that account for 85% of the participating mass associated with Ux, Uy, and Rz degrees of freedom. Standard codes allow the adoption of this simplified approach considering uncertainties in seismic load distribution.

4. Overview of the case studies

The optimization detailed in Section 3.2 is applied to different Case Studies through the algorithm illustrated in Fig. 1. Each Case Study represents a RC building to be retrofitted for which an inter-story drift threshold is defined. Three buildings are analyzed, each exhibiting a distinct level of complexity concerning the total number of potential exoskeletons to be located and different in-plan irregularities. The six inter-story drift thresholds ($\frac{H_{story}}{\beta}$) defined in Section 3.1, associated to light damage, are analyzed for each building.

The case studies are named CS1, CS2, and CS3, representative of three different building typologies, each of these subjected to the mentioned-above ISD thresholds range. The parameters selected for the optimization of each Case Study are presented in Table 3 in terms of quantity of design variables, population size, and number of iterations, along with the main characteristics of the corresponding unretrofitted buildings. It is worth noting that a realistic critical safety threshold equal to 0.9 is assumed for the demand–capacity ratio (DCR).

4.1. Vulnerable system: Existing building

The present research examines no.3 three-dimensional moment-resisting reinforced concrete (RC) buildings. Case studies were designed with the objective of analyzing buildings representative of the civil built environment and designed with outdated seismic standards. The beams and columns are realized with C35/45 concrete and B450C steel rebars, and their cross-sections and reinforcement details are provided in Table A.5 for each building. The elements are fully restrained to each other, the columns are fully restrained to the foundation system, and rigid diaphragms were adopted on each floor to simulate the in-plane effect of the slabs.

The structural verifications for the design of the buildings were conducted following the Italian standard NTC 18 [48]. These buildings were designed to be safe under the Ultimate Limit State for gravitational loads, but they do not meet the current seismic standards. A significant proportion of the elements in each building do not comply with the structural verifications when facing seismic action. Specifically, in all the investigated case studies, almost 85% of structural elements are not safe under horizontal loads, with safety factors lower than 0.5 for some elements of the vulnerable system. In Table 3, the characteristics of the unretrofitted buildings are provided, in terms of the number of critical elements (DCR over 0.9), maximum and average Demand–Capacity Ratio (DCR), initial top displacement, and inter-story drift, along with the parameters' setting adopted for the optimization processes of each.

Fig. 2 depicts the geometry of the buildings and the location of the stairs, along with all potential exoskeleton positions. The modules are 5 m × 5 m, with the exception of Case Study 2, in which the general modules are 7 m × 5 m and the modules in which the stairs are located are 5 m × 5 m. All the buildings have 3 stories of 4 m each, resulting in a total height of 12 m. The structures' geometries and the position of the stairs have been selected in order to incorporate different behaviors in X and Y directions, in-plan irregularities, and torsional effects.

Permanent and non-permanent loads accounting for structural and non-structural elements as well as live loads are defined as follows: the dead load G_1 equal to the weight of the beams and columns plus 3 kN/m^2 to account for the weight of the slabs, the permanent load G_2 equal to 2 kN/m^2 for the screed and partitioning walls, the façade permanent load G_3 equal to 10 kN/m, and the live load Q equal to 3 kN/m^2.

For the definition of the seismic action, the buildings are considered to be located in Foggia, Italy (B soil type) and the analyses are conducted for the Life Safety Limit State. For these conditions, the peak ground acceleration a_g/g is equal to 0.1337 and the acceleration that corresponds to the *plateau* of the response spectrum is $0.42g$. The response spectrum is presented in Fig. 3, where the fundamental periods of the RC buildings in X and Y directions are highlighted. Based on these periods, it can be observed that all the structures are characterized by a higher stiffness in the X direction than in the Y direction.

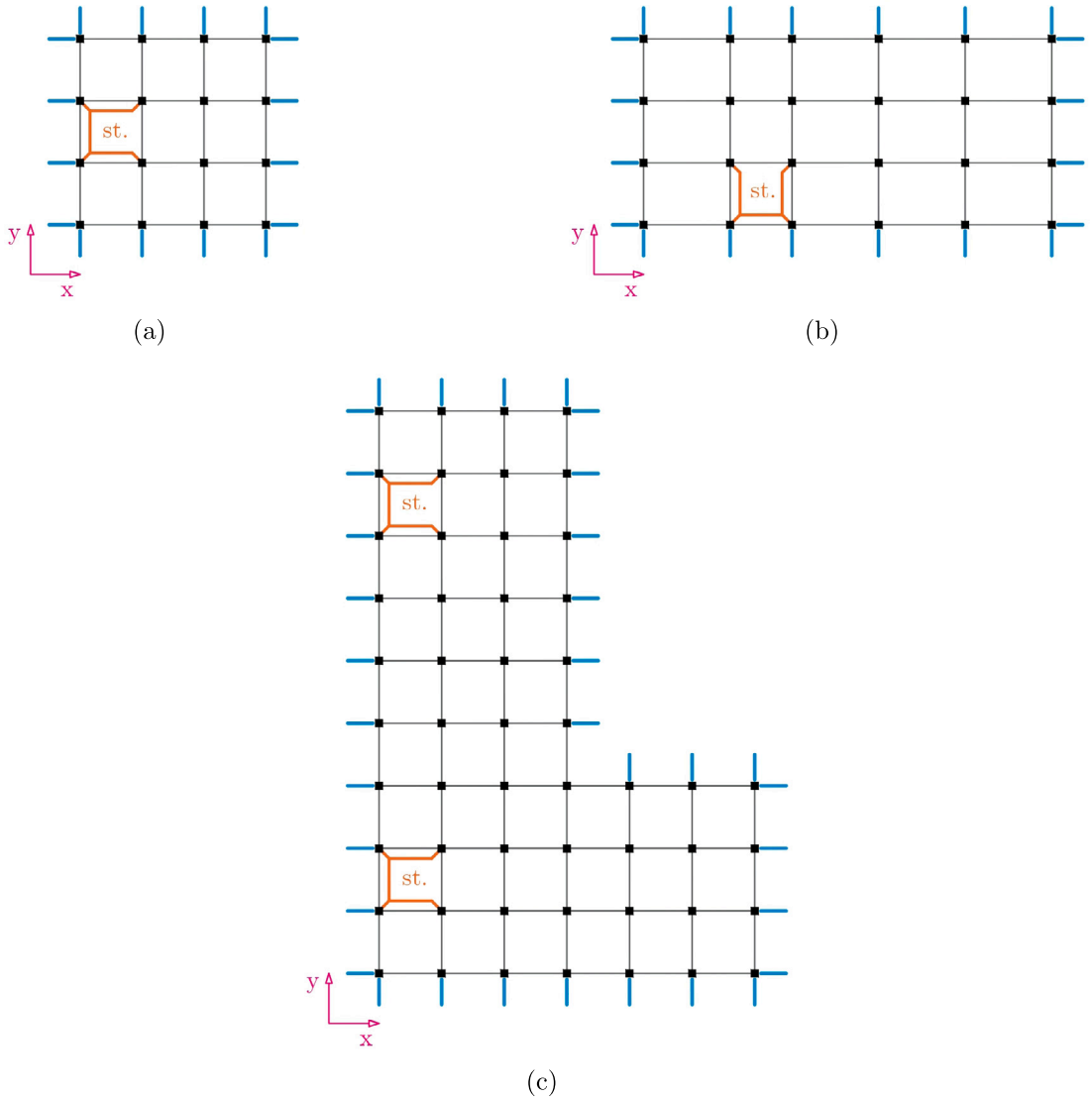

Fig. 2. Top view of the buildings of (a) CS 1, (b) CS 2, (c) CS 3, with stairs (st.) (orange) and all potential exoskeletons (blue). (For interpretation of the references to color in this figure legend, the reader is referred to the web version of this article.)

4.2. Retrofitting system: Exoskeletons layout

The exoskeletons under consideration for this study are non-dissipative two-dimensional steel frames, oriented perpendicular to the building façade. The definition of the hinges and connection typology is illustrated in Fig. 4.a. Exoskeletons feature an internal column in close proximity to the building and an external column located at a distance of three meters from the internal one. The columns are continuous in height and hinged at the base, thereby enabling them to function under reduced moment stresses. The exoskeletons' beams are aligned with the building's floors and are continuously connected to the columns, and each story has bracing systems that are hinged at both ends.

The exoskeletons are connected to the column-beam nodes of the existing building through connections that are hinged at both ends (see Fig. 4.a), enabling rotation in the plane of the exoskeleton. This design allows collaboration between the exoskeletons and the existing structure in resisting horizontal actions while avoiding the generation of tensile stresses on the building's columns.

The described configuration was selected over the one illustrated in Fig. 4.b. The non-selected configuration presents fully restrained connections between the exoskeleton and the building and all the columns are hinged at both ends. These characteristics result in a reduction in the overall weight of the final design, due to the enhanced coupling with the building and the higher stiffness presented by the exoskeletons. However, because of the fully-restrained connection with the exoskeletons, the building's columns experience non-acceptable tensile stresses resulting in cracking and irreparable local failure which compromise the structural safety

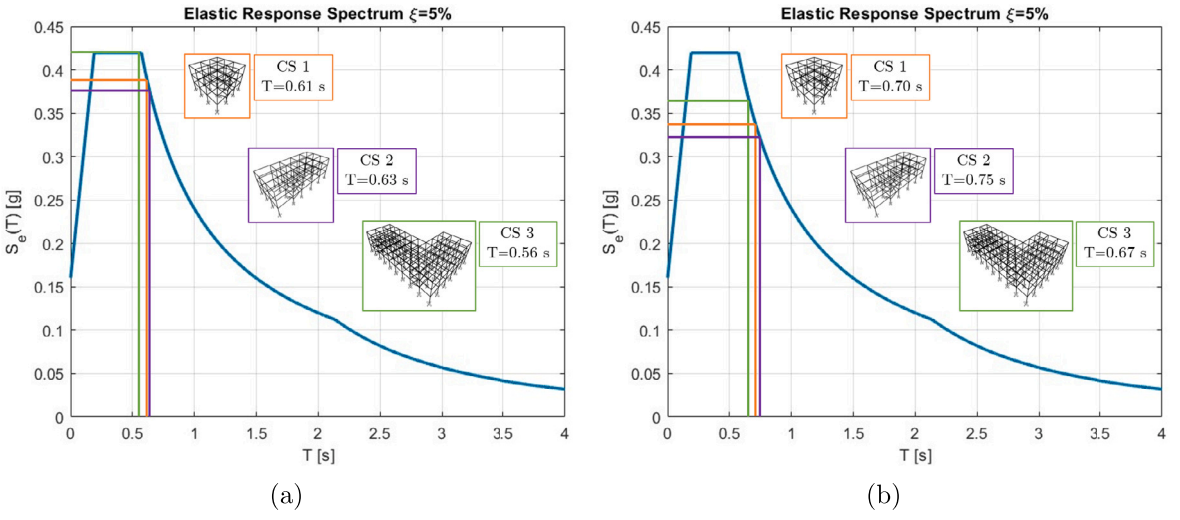

Fig. 3. Elastic response spectrum of Foggia, Italy and fundamental periods for each Case Study in (a) X and (b) Y directions.

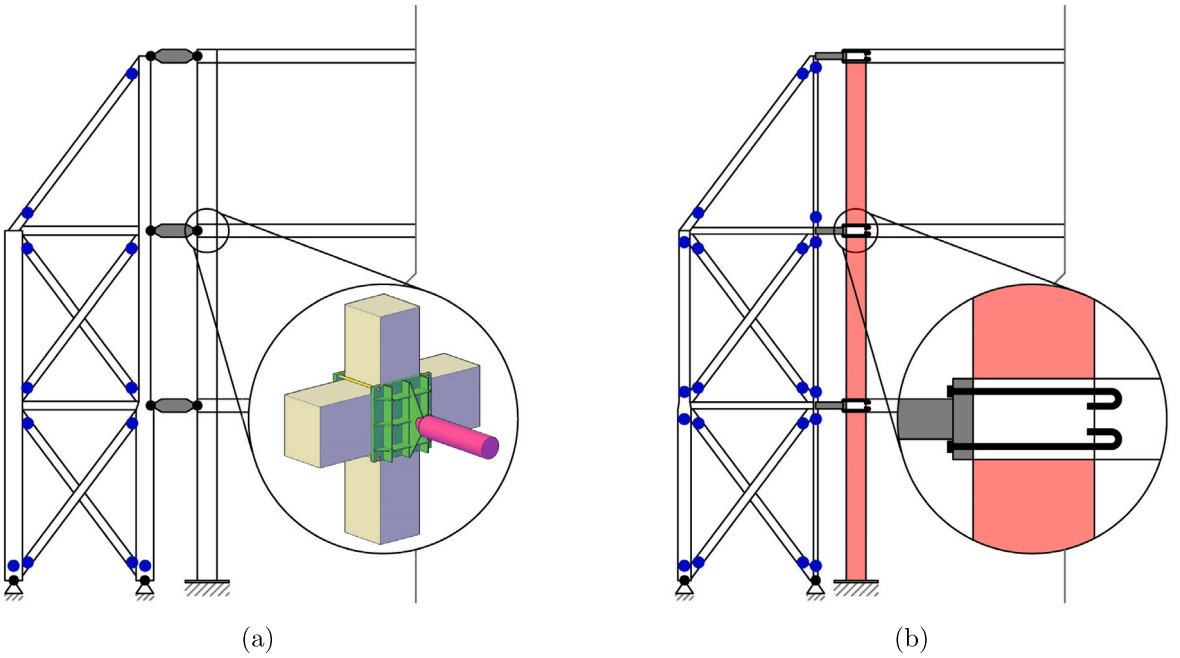

Fig. 4. Exoskeleton layout and definition of hinges (in blue) and connection typology of the (a) hinged configuration (selected) and (b) fully restrained configuration (not selected). All structural members depicted in the Fig.s are in scale. (For interpretation of the references to color in this figure legend, the reader is referred to the web version of this article.)

of the building. Additionally, this specific type of connection requires special attention during the construction phase that can hardly be realized in practice because of the existing steel rebars at the beam–column joint. For all these reasons, configuration 4-a was effectively implemented into the structural model as the most realistic and feasible solution from an engineering point of view.

The elements of the exoskeletons are standard Circular Hollow Sections (CHS) realized with S355 steel. The cross-sections are selected through the optimization procedure from a list of standard profiles according to the European code EN10219-2. Fig. 5 illustrates the geometric layout of the exoskeletons and the grouping of the elements performed for the optimization. Moreover, the design of exoskeletons is assumed to be the same for each independent retrofitting system resulting in a total number of Size DVs equal to 9.

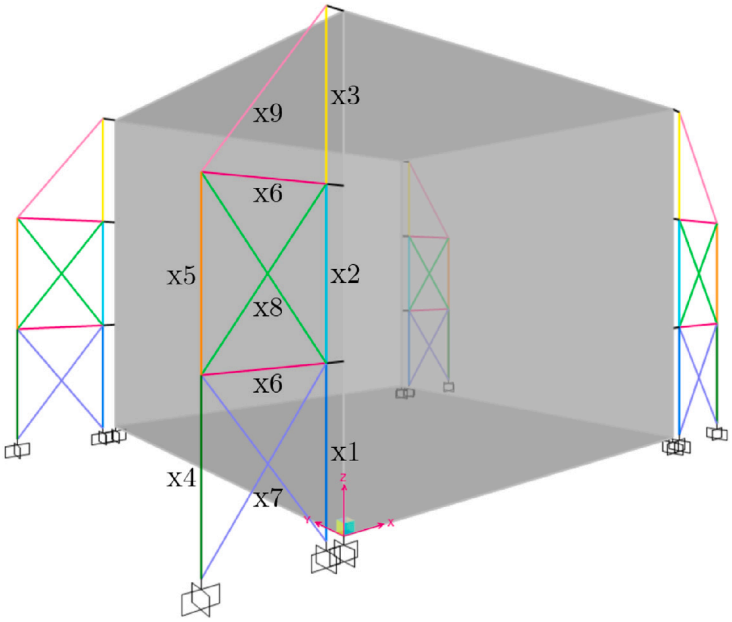

Fig. 5. View of the exoskeletons layout and detail of the element grouping for the size optimization with corresponding Design Variables (x#).

5. Results and interpretation

The performance-based optimization process described in Section 3 was applied to the case studies presented in Section 4 to determine the optimal retrofit realized by steel exoskeletons. These final configurations are identified by an optimal number of exoskeletons, their positions around the building, and the sizing of their elements. An optimal solution was obtained for each combination of a building and an inter-story drift threshold, resulting in a total of eighteen configurations. This section aims to give a clear interpretation of the (i) principles behind the spatial arrangement of exoskeletons (Section 5.1), (ii) main trend of the optimization OF and constraints' (Section 5.2), and (iii) structural response of the coupled system (Section 5.3).

5.1. Optimal exoskeleton configurations

The resulting configurations are presented in Figs. 6, 7, and 8, for Case Studies 1, 2, and 3, respectively, and the optimal cross-sections of the exoskeleton elements are presented in Table A.6 for the designs obtained for the inter-story drift threshold of H/650, which represents the most restrictive and steel-demanding case. In order to interpret these images, it is necessary to consider the position of the exoskeleton in terms of two main characteristics. The first one is the main direction in which they provide an increase in stiffness, that is their in-plane direction, having little influence in their out-of-plane direction. The second characteristic is the distance between the exoskeleton and the center of stiffness of the building, measured perpendicular to the in-plane direction. This distance allows the exoskeleton to modify the position of the center of stiffness of the system, bringing it closer to the center of mass and thus reducing the torsional response of the building. For instance, the spatial configuration of the solutions obtained for CS1 with H/450 and H/500 (see Fig. 6.b and .c) are to be considered equal from this point of view.

In the considered buildings, the center of stiffness is located in close proximity to the staircase. Consequently, more exoskeletons are located in the most distant locations to it, which experience the greatest displacements. This approach aims to bring the center of stiffness closer to the center of mass of the building and to generate forces with greater arms to counteract the global torsional effects. In contrast, in the direction of symmetry of the building, as in the X direction for CS1, the exoskeletons are positioned symmetrically with respect to the symmetry axis.

Another interesting outcome came from the optimal configuration of exoskeletons regarding the number of exoskeletons positioned in each direction, especially considering that all exoskeletons in a given configuration are equal among them. As illustrated in Fig. 3, all three buildings exhibit higher stiffness in the X direction than in the Y direction. Consequently, the majority of resulting configurations are characterized by a greater number of exoskeletons positioned in the weaker direction of the building (Y).

Furthermore, it can be appreciated that the number and positions of exoskeletons vary with the inter-story drift threshold. Such variability is attributable to both the optimization process's discrete nature and the structure's changing stress distribution according to the retrofitting system's increasing stiffness associated with more restrictive inter-story limits. In other words, the section of each element is selected from a standard section list, therefore, during the optimization process, the quantity of exoskeletons is dynamically adjusted in order to use the steel profiles that better suit the requirements. Subsequently, alterations in the number of

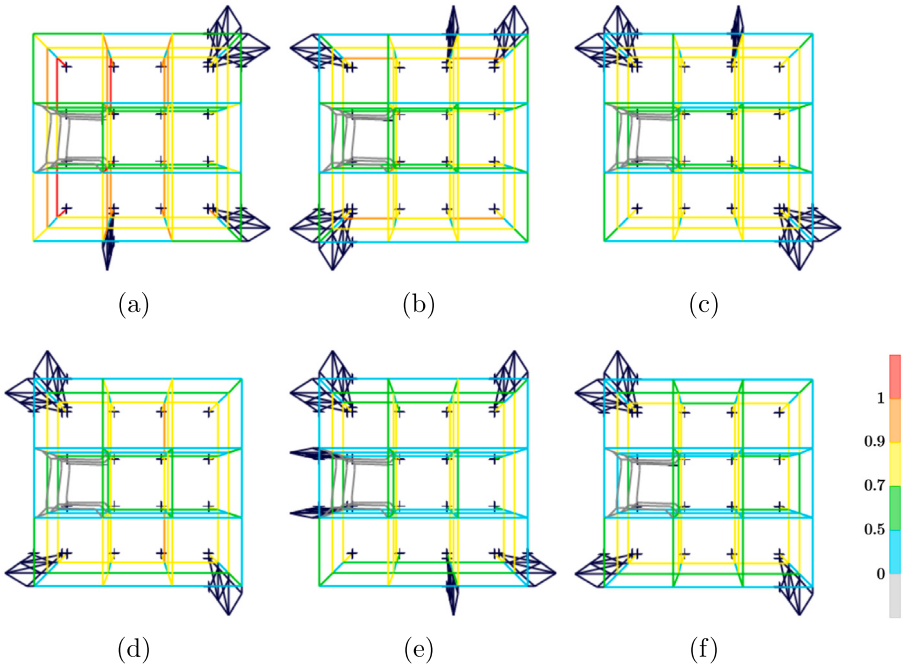

Fig. 6. Optimal solutions obtained for Case Study 1 with inter-story drift thresholds of (a) H/400, (b) H/450, (c) H/500, (d) H/550, (e) H/600, and (f) H/650; and color map of the structural verifications performed according to the NTC18. (For interpretation of the references to color in this figure legend, the reader is referred to the web version of this article.)

exoskeletons result in changes to their positions, in order to readjust the distribution of added stiffness. The complexity of all these structural behaviors and design criteria, which simultaneously occur at each analysis of each individual along all the iterations of the optimization process, are efficiently managed by the algorithm that is able to provide unpredictable solutions so far from the design obtained following previous experience or design thumb rules.

Nevertheless, despite the existence of variability in the solutions obtained for a given building, the aforementioned principles that govern the spatial distribution of exoskeletons remain consistent across all configurations.

5.2. Overview of the OF and constraints trends

Focusing on the parameters that guide the optimization process, Fig. 9 illustrates the final values of incidence, Inter-Story Drift Ratio (ISDR) (Eq. (4)), and Demand–Capacity Ratio (DCR) (Eqs. (5) and (6)) corresponding to each optimal result. These values are plotted against the ISD threshold used as a dominant parameter constraint for each case, from the most permissive one, H/400, to the most demanding one, H/650.

As expected, the incidence of the solutions, in terms of weight of steel per square meter of building, increases as the ISD limit becomes more restrictive. On the other hand, the optimization tool manages to obtain solutions with ISDR equal to 1 in each case, complying perfectly with the different imposed thresholds (note that CS1, CS2 and CS3 ISDR are overlapped in Fig. 9). Conversely, the mean of the exoskeleton elements' DCR, evaluated as the average among the DCR values of all the exoskeletons' members, decreases as the threshold becomes more demanding. This occurs because the selection of the exoskeleton's sections is guided by the objective of providing enough stiffness to the system to comply with the allowable ISD. As the ISD threshold decreases (lower value of allowable displacement), the stiffness required to control the ISD increases, and the DCR is satisfied with greater ease. However, independently of the threshold limits, the displacement parameter control ISDR dominates the design of exoskeletons.

As proof of the benefits deriving from the proposed approach, the authors make a comparison between the steel demand of traditional stiffness-ratio-based designs (K_{ratio} = 6.67) with that of the optimal configurations obtained through the performance-based approach. The comparison is conducted for all three buildings, for an inter-story drift (ISD) threshold of H/650, which represents the most restrictive and steel-demanding case.

As illustrated in Fig. 10, the performance-based optimization approach results in a substantial reduction in the required steel weight for the retrofit. The results indicate that the proposed approach achieves a 65% reduction in required steel, corresponding to only one-third of the steel required for conventional stiffness-ratio-based designs. This significant material efficiency is achieved while maintaining a high level of structural safety, as demonstrated by the Demand–Capacity Ratios (DCRs) across all buildings. The maximum DCR observed among all structural elements is 0.86, while the average DCR remains at 0.53, indicating that, in the design obtained through the performance-based approach, all elements comfortably satisfy structural verification requirements.

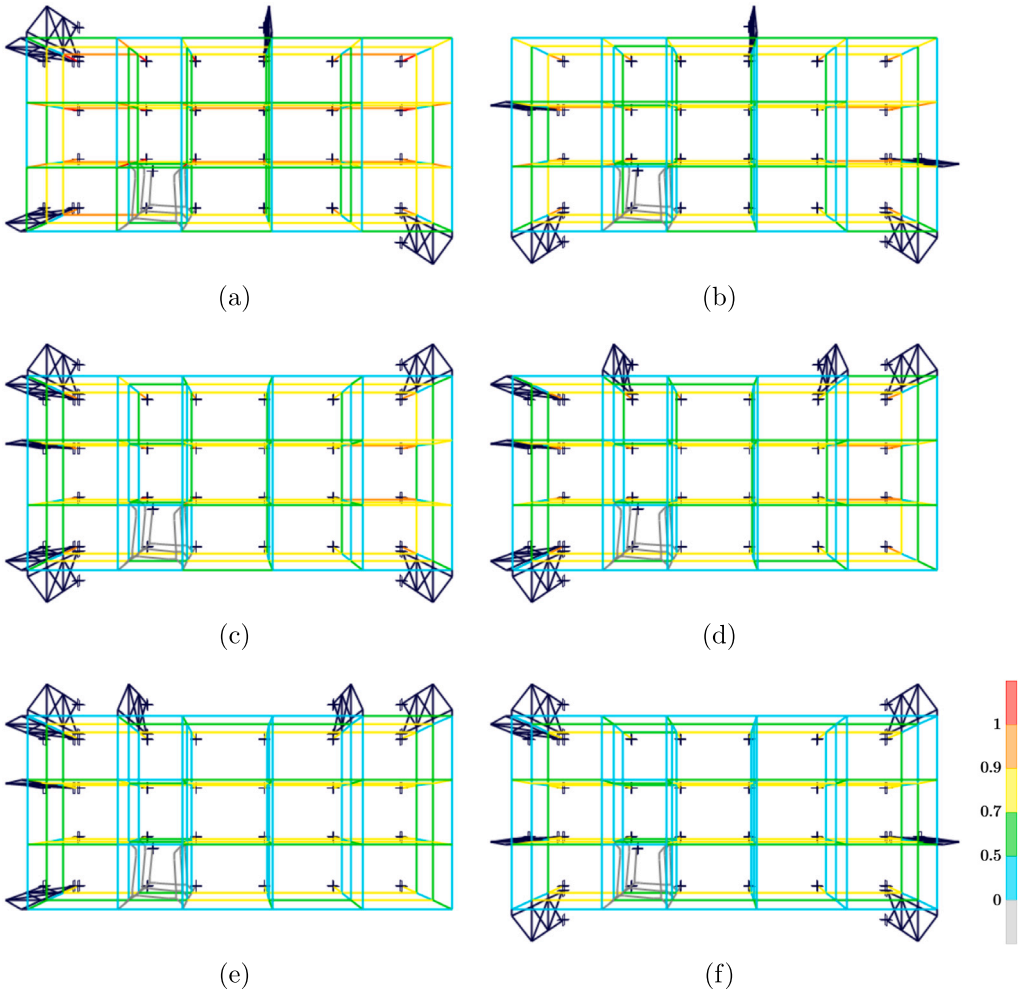

Fig. 7. Optimal solutions obtained for Case Study 2 with inter-story drift thresholds of (a) H/400, (b) H/450, (c) H/500, (d) H/550, (e) H/600, and (f) H/650; and color map of the structural verifications performed according to the NTC18. (For interpretation of the references to color in this figure legend, the reader is referred to the web version of this article.)

5.3. Unloading effect and stiffness ratio of the coupled system

The incorporation of exoskeletons into the system leads to an increase in stiffness resulting in an increase in seismic actions, in addition to a regularization of natural vibration periods. Nevertheless, a significant proportion of the seismic force is absorbed by the exoskeletons, thereby unloading the building, as illustrated in Fig. 11.

The substantial unloading of the building resulted in a notable improvement in the structural verification of the elements, as also testified by the color map illustrations of the Demand–Capacity Ratios illustrated in Figs. 6, 7, and 8.

On the other hand, the observed unloading effect is clearly explained by the stiffness ratio of the coupled system. The stiffness ratios were determined as the ratio between the horizontal stiffness of the exoskeletons and the one of the original building alone, for each of the eighteen cases and in the X and Y directions. For this study, the ratio between the base shear taken by the exoskeletons and by the building is selected as indicator of their stiffness, given that the system operates within the elastic field, and thus, dynamic linear analyses can be exploited to assess the structural behavior of the system with a high level of accuracy.

The resulting stiffness ratios are presented in Fig. 12 as the mean value between those corresponding to the X and Y directions. It can be appreciated that the stiffness ratios increase with the decrease in the permitted inter-story drift. The observed variability in the trend can be attributed to the discrete nature of the optimization process, which relies on a list of standard CHS profiles for the exoskeletons' sizing.

The main outcome resides in the obtained stiffness ratios which are significantly below the threshold provided in the standard regulations. Focusing on the solutions that provide zero critical elements in the retrofitted building, the stiffness ratios are 1.17, 1.29, and 0.77, for Case Studies 1, 2, and 3, respectively. In other words, exoskeletons designed with 1.17, 1.29, and 0.77 times the horizontal stiffness of the building lead to structures with zero critical elements. A comparison of these values with the 6.67

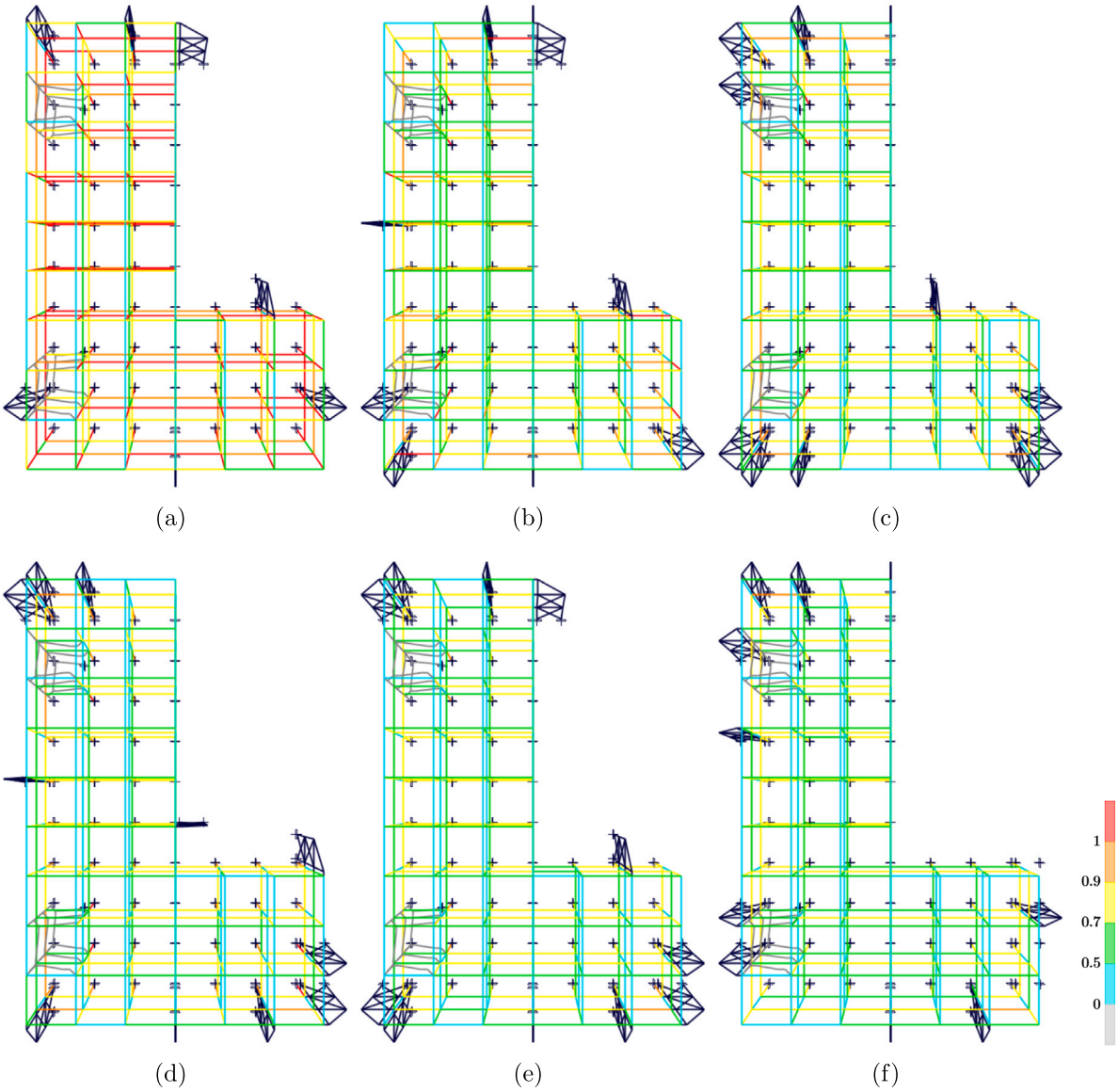

Fig. 8. Optimal solutions obtained for Case Study 3 with inter-story drift thresholds of (a) H/400, (b) H/450, (c) H/500, (d) H/550, (e) H/600, and (f) H/650; and color map of the structural verifications performed according to the NTC18. (For interpretation of the references to color in this figure legend, the reader is referred to the web version of this article.)

provided by the Italian and European Standard Regulations, NTC 18 [48] and Eurocode 8 [49], reveals a significant reduction. This reduction indicates that the performance-based approach provides solutions that require a stiffness of the exoskeletons between 19% and 11% of that proposed by the standard codes, by assuming a collaborative behavior of the vulnerable system and the retrofitting one. Moving away from the distinction of primary and secondary elements, an efficient design of the exoskeletons is obtained by exploiting the residual capacity to resist horizontal actions of the existing building.

Both Figs. 12–14, should clarify the implications of stiffness reduction into the actual safety margin. Complying with the assumed hazard level, well-defined inter-story thresholds ensure acceptable safety margins of the existing building after the intervention. This is accomplished by exploiting the residual capacity of the existing building (in the elastic field) and due to the stiffness contribution provided by the exoskeletons.

6. A simplified approach to consider non-linear effects

To ensure the validity of the linear dynamic analyses adopted in this study, additional analyses were conducted, particularly focusing on potential non-linear behaviors that may develop in the structure under seismic loading. Since the imposed inter-story

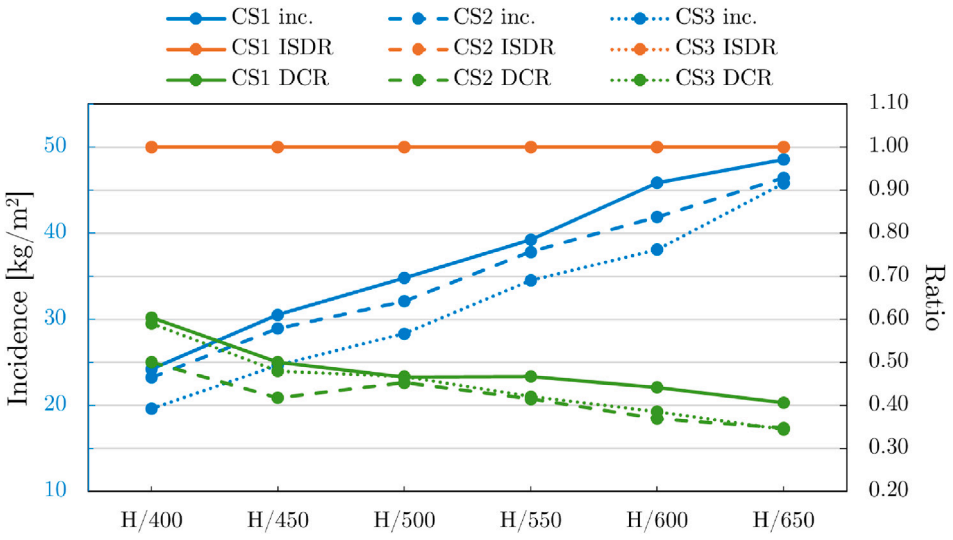

Fig. 9. Final values of incidence (steel weight per square meter of building), Inter-Story Drift Ratio (ISDR), and mean Demand–Capacity Ratio (DCR) of the exoskeleton's elements, against the inter-story drift threshold (H/#) for each building (CS #).

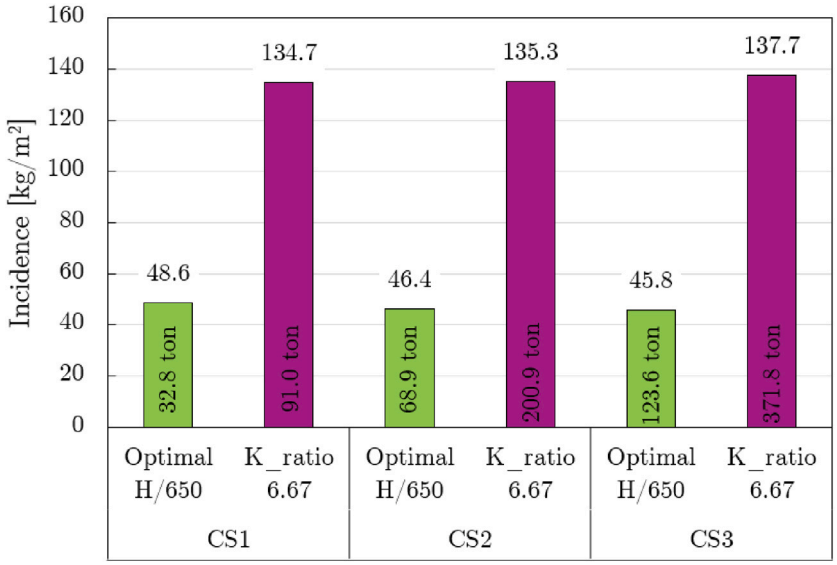

Fig. 10. Comparison of the incidence of steel for the optimal exoskeleton configurations for the inter-story drift threshold of H/650, with that corresponding to a traditional stiffness-ratio-based design with $K_{ratio} = 6.67$. Expressed in weight of steel per unit area of building, and in total steel weight.

drift (ISD) thresholds were established to control structural damage, and since these limits correspond to *light damage* (see Table 2), the system is expected to remain within the elastic range. Consequently, the yielding of the steel and the ultimate compressive strength of the concrete are not reached. In this case, linear dynamic analyses are valid and accurate for this application.

To explicitly verify the structural behavior under increasing lateral loads, non-linear static (pushover) analyses were performed on the optimal exoskeleton configurations obtained through the design process. As an example, the pushover curves presented in Fig. 13 correspond to the CS3 case with an ISD threshold of H/400, which is the most critical case. These curves illustrate the base shear vs. displacement response in both the X and Y directions. The results confirm that the system remains entirely within the elastic range along the entire loading history with no formation of plastic hinges. Consequently, the resulting displacements, stresses, and distribution of horizontal forces between the exoskeletons and the building are equal either performing linear dynamic analyses or pushover analyses.

While the pushover analyses confirmed that no plastic hinges develop, non-linear effects related to concrete cracking under flexural stresses must still be addressed. Specifically, although the steel reinforcement remains below its yield stress, the cracking of concrete in tension leads to stiffness degradation in the RC elements resulting in a significant change in the load distribution

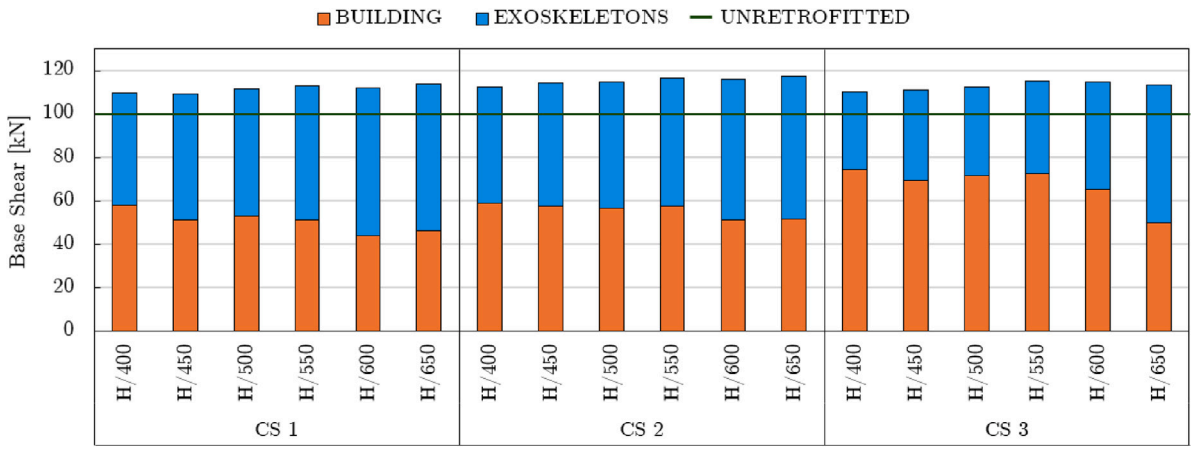

Fig. 11. Proportion of base-shear borne by the building and the exoskeletons, compared to that of the unretrofitted building (100%), which is 2380 kN for CS 1, 4939 kN for CS 2, and 8853 kN for CS 3.

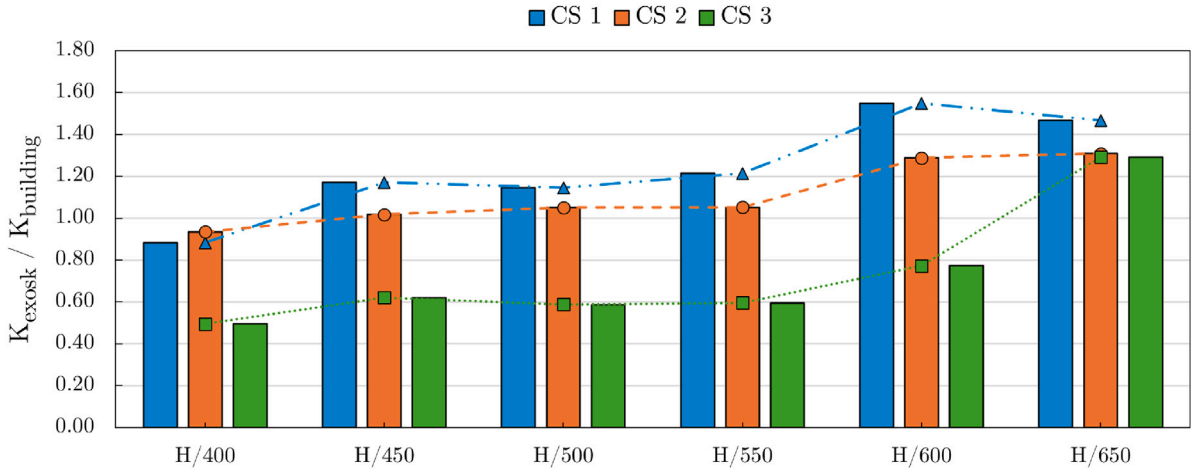

Fig. 12. Stiffness ratios as the mean value between those corresponding to the X and Y directions, for each Case Study (CS #) and ISD threshold (H/#).

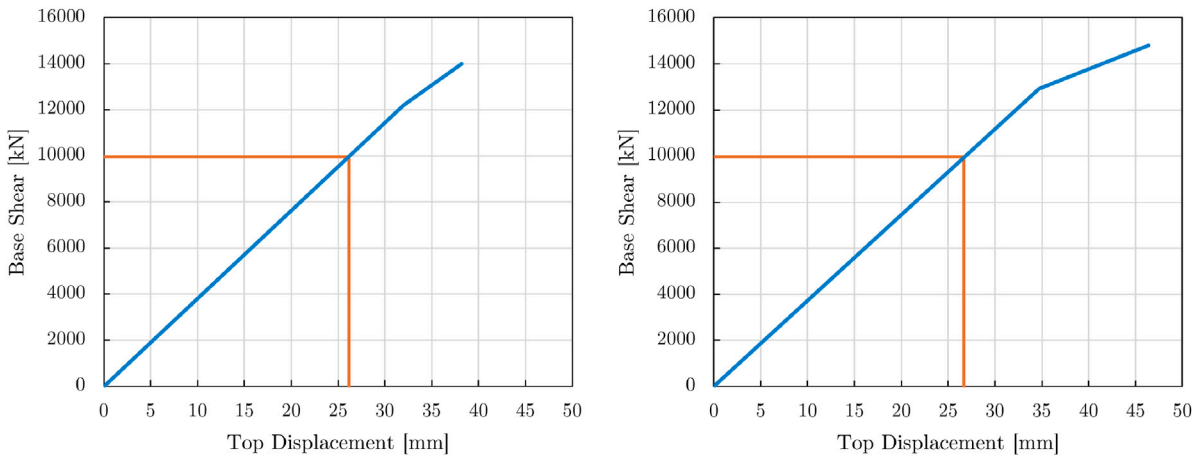

Fig. 13. Pushover curves (Base Shear vs. Top Displacement) for CS3 with ISD threshold of H/400, in (left) X and (right) Y directions. The static equivalent seismic load level and corresponding displacement are highlighted in the curves.

Table 4
Results of progressive degradation of the building and related reduction of stiffness, for CS 3 with H/600, in terms of: proportion of base-shear borne by the building and exoskeletons in each direction ($\%V$), and respective stiffness ratios (K_{ratio}), along with the Demand–Capacity Ratios (DCR) of the exoskeleton elements (maximum and average) and the building's elements (maximum).

%K	$\%V^X_{str}$	$\%V^Y_{str}$	$\%V^X_{exk}$	$\%V^Y_{exk}$	K^X_{ratio}	K^Y_{ratio}	DCR^{exk}_{max}	DCR^{exk}_{avg}	DCR^{str}_{max}
1	61.6	52.0	38.4	48.0	0.62	0.92	0.81	0.39	0.95
0.90	59.0	49.5	41.0	50.5	0.69	1.02	0.86	0.41	0.91
0.80	56.1	46.8	43.9	53.2	0.78	1.14	0.91	0.42	0.85
0.70	52.8	43.6	47.2	56.4	0.89	1.29	0.98	0.44	0.80
0.60	48.9	40.0	51.1	60.0	1.05	1.50	1.05	0.46	0.76
0.50	44.3	35.8	55.7	64.2	1.26	1.79	1.14	0.49	0.71
0.40	38.8	31.0	61.2	69.0	1.58	2.23	1.25	0.51	0.66
0.30	32.1	25.3	67.9	74.7	2.11	2.96	1.37	0.55	0.60
0.25	28.2	22.0	71.8	78.0	2.54	3.54	1.45	0.56	0.57
0.25[a]	24.6	18.9	75.4	81.1	3.06	4.29	0.96	0.48	0.57

[a] In this case, the non-verified exoskeleton elements have been replaced.

between the two structural systems. To assess this phenomenon, a parametric analysis was conducted by progressively reducing the stiffness of the existing RC building and evaluating the redistribution of forces between the building and the exoskeleton system.

For this purpose, the stiffness of the RC structure was reduced in steps down to one-quarter of its original value, representing a conservative estimate of stiffness loss due to cracking. At each degradation step, the proportion of horizontal seismic action carried by the RC structure and the exoskeletons was determined, and the stiffness ratio was determined as the ratio between the respective percentages: $K_{ratio} = {}^{K_{exosk}}/_{K_{building}}$. Additionally, the Demand–Capacity Ratios (DCRs) of both the exoskeleton elements and the RC members were evaluated at each stage.

The results of this study, presented in Table 4, correspond to CS3 with an ISD threshold of H/600, which was selected as a representative case. As expected, the progressive reduction in the stiffness of the RC structure leads to an increase in the share of lateral forces carried by the exoskeletons. Thus, the progressive increase in K_{ratio} is given by the decline in $K_{building}$, while K_{exosk} remains constant. However, despite a significant reduction in the RC stiffness (up to 75%), the required resistance of the exoskeletons does not increase proportionally. The average DCR of the exoskeleton members rises moderately from 39% to 56%, demonstrating that the optimized exoskeleton configuration maintains structural efficiency even under significant stiffness degradation.

In the final degradation stage, some exoskeleton members exceeded their capacity, particularly bracing elements at the first floor. To address this, a minor increase in the cross-section of these elements was introduced, leading to a negligible increase in the total exoskeleton mass ($102.8t$ to $103.9t$). This minor adjustment ensured that all structural members remained within their capacity limits while preserving the overall efficiency of the system.

These findings confirm that, because of the limitation to the structural damage, the system remains in the elastic field. This reflects the validity of the performed linear analyses and indicates that the differences between the results of linear and non-linear analyses are either null or negligible for this application.

7. Safety level assessment through sensitivity analysis

Until now, the authors focused on demonstrating the validity of the proposed philosophy as a promising alternative to the traditional approach recommended by Standard codes. However, as observed in the previous sections, color map representation of the structural verification depicted in Figs. 6–8 show a significant variability on the safety level for each different building typology and assumed ISD thresholds. In fact, it is worth noting that no safety levels (e.g. maximum stress expected at each member of the RC building) have been included as constraints of the optimization framework. In other words, the ISD thresholds, explicitly included as constraint parameters in the performance-based approach, are indirectly responsible for the effective level of stress of the RC elements composing the existing building.

For instance, at least one optimized configuration among all the investigated case studies exhibits certain amount of RC elements with a DCR over 0.9 which should be reasonably assumed as critical, on the premise that these elements should be subject to local interventions (see Figs. 6.a, 7.a and 8.a). Based on this, the authors conducted a sensitivity analysis aiming to classify the optimized solution obtained for different inter-story thresholds in terms of level of safety and goodness of the retrofitting system. A *criticality* index was defined as the ratio between the number of critical elements after the retrofit and the same number before the retrofit.

The relationship between the criticality and the incidence of the optimal configurations is represented in Fig. 14. The curves illustrate the trade-off between the number of elements that would require local interventions (#LI) and the incidence representative of the exoskeletons' cost. Moreover, the ISD threshold corresponding to each point can be identified by the markers, and the color map representation of the structural verifications for CS3 with $H/400$ and $H/650$ ISD thresholds are presented as examples of the extremes of the curves.

In this figure, different zones have been distinguished illustratively. These zones correspond to varying amounts of elements that remain critical after the introduction of the exoskeletons and necessitate local interventions. Based on the experience of the authors, high criticality zone was assumed to collect all the final configurations characterized by a number of critical elements over 20%. In this case, the retrofitting approach is not able to guarantee structural safety resulting in local interventions of a significant portion

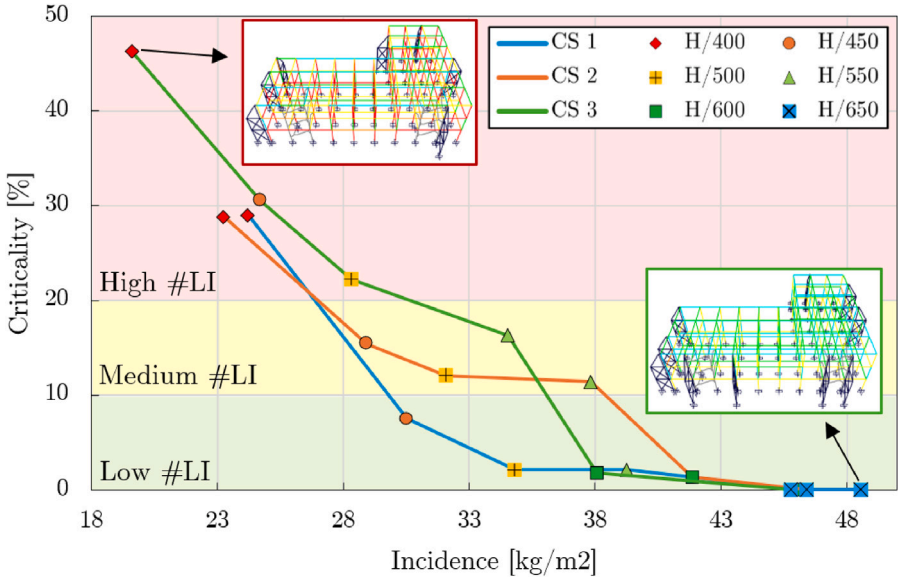

Fig. 14. Criticality, in terms of the ratio between the number of RC elements in the retrofitted building with DCR over 0.9 and that in the unretrofitted building, against Incidence, in terms of weight of steel by area unit of the building; and illustrative zones corresponding to the required number of local interventions (#LI); for each Case Study (CS #) and each ISD threshold (H/#). (For interpretation of the references to color in this figure legend, the reader is referred to the web version of this article.)

of the existing building's elements. In the same way, medium and low criticality zones were identified according to an acceptable number of critical elements included in the range of 10%–20% and lower than 10%, respectively.

Firstly, the designer can establish an admissible number of local interventions (#LI) to be performed inside the building complying with the economic budget and their technical practicability. Subsequently, the most convenient inter-story drift threshold for the design can be defined according to the lowest incidence of steel resulting in the most efficient and sustainable retrofitting design. As expected, almost all the retrofitting configurations lying beyond the high criticality level are obtained for the less restrictive threshold limits. The displacement limits of $H/450$ for CS1 and CS2 and $H/550$ for CS3 provide the first optimized retrofitted solutions with an acceptable level of criticality associated with a sustainable increase in the incidence.

8. Conclusions

In the current context, steel exoskeletons offer significant advantages for the seismic retrofitting of RC buildings. However, their application is constrained by the high cost associated with their oversized design. This is a consequence of the provisions of certain standard codes that require a minimum horizontal stiffness of the exoskeletons.

In this paper, an alternative approach was adopted for the optimal design of exoskeletons, based on the control of the inter-story drift (ISD) associated to proper damage levels of the existing building. The design was conducted through an optimization process with the objective of minimizing structural weight while incorporating the ISD threshold and the structural verifications of the exoskeletons as constraints. This process determined the optimal number of exoskeletons and their positions around the building, as well as their optimal sizing. Additionally, different admissible ISDs were analyzed through a sensitivity analysis, and valuable insight regarding the influence of this displacement control parameter on the structural safety of the buildings as well as the design of the retrofitting system are introduced. The selected case studies encompass three RC buildings representative of the built environment, exhibiting diverse complexities, in-plane irregularities, and dimensions of the optimization problem demonstrating the strong versatility of the proposed automatic design of such a retrofitting system. This process yielded an optimal configuration for each combination of a building and ISD threshold.

The analysis and comparison of these configurations resulted in key findings on the achieved performances for solutions with varying amounts of steel required. Once the main mechanical principles governing the optimal arrangement of the exoskeletons were identified, the structural behavior of the obtained systems was studied. For each optimal configuration, the structural performance of the coupled system was evaluated according to the Italian standards NTC 18. The results of the sensitivity analysis demonstrated the influence of the selected ISD threshold on the level of safety and on the quantity of critical RC elements in the retrofitted building. Moreover, it was possible to assess the trade-off between the criticality of the building and the incidence in terms of mass of steel per unit area of building.

Ultimately, the stiffness ratios of the optimal solutions were determined as the ratio between the horizontal stiffness of the exoskeletons and that of the building. The stiffness ratios obtained through the performance-based design are significantly lower than those recommended by current standard regulations. Specifically, the stiffness ratios of the solutions that guarantee the

Table A.5
Cross-section and reinforcement details on the Reinforced Concrete elements of the case studies (CS#), regarding columns at the 1st, 2nd, and 3rd floors, and beams in the X direction (primary) and Y direction (secondary). For the beams, the number of reinforcement bars is expressed as top + bottom.

	CS1		CS2		CS3	
	Section [cm]	Reinforcement [n.bars ϕ mm]	Section [cm]	Reinforcement [n.bars ϕ mm]	Section [cm]	Reinforcement [n.bars ϕ mm]
Columns 1	45×45	$8\,\phi\,24$	50×50	$12\,\phi\,24$	50×50	$12\,\phi\,24$
Columns 2.	40×40	$8\,\phi\,24$	45×45	$12\,\phi\,24$	40×40	$12\,\phi\,20$
Columns 3	35×35	$8\,\phi\,20$	40×40	$12\,\phi\,20$	35×35	$8\,\phi\,20$
Beams X-dir	30×45	$4 + 4\,\phi\,24$	40×60	$6 + 6\,\phi\,24$	40×50	$5 + 5\,\phi\,24$
Beams Y-dir	30×40	$4 + 4\,\phi\,20$	30×45	$4 + 4\,\phi\,24$	30×50	$5 + 5\,\phi\,20$

absence of critical elements in the retrofitted buildings were 1.17, 1.29, and 0.77, for the different case studies in contrast with the recommended value of 6.67 specified by the NTC 18 and Eurocode 8. This reveals a reduction of between 80% and 90% in the required stiffness, which translates into a reduction of 65% of required steel in the most steel-demanding configurations. Accordingly, the exoskeletons should exhibit a stiffness that is approximately equal to that of the existing building, overcoming the definition of primary and secondary elements proposed by the standard regulations. These results highlight the key role of an efficient collaborative behavior between the building and the exoskeletons to resist the seismic action, without over-relying on excessively stiff exoskeletons. This collaborative behavior derives from well-defined displacement thresholds that guarantee the structural safety of the building and the achievement of the expected performance level.

In conclusion, this study proposes a paradigm shift in steel exoskeleton design, focusing on a performance-based approach over traditional stiffness ratio control. The findings underscore the potential for more cost-effective and structurally efficient retrofitting solutions, thereby making steel exoskeletons a more attractive option for seismic retrofitting of buildings while simultaneously encouraging sustainable design approaches through conscious resource exploitation in the construction sector.

Limitations of the proposed approach mainly refer to the limited number of investigated case studies, which need to be expanded to confirm the research results. In future works, further validations of these findings across a broader range of building typologies (e.g. variations in geometry, tall buildings), alternative materials (e.g. timber, aluminum), and seismic conditions are necessary to ascertain the practical applications of this approach and reach new insights in the field of cost-effective and sustainable optimal design of such retrofitting systems. Additionally, future efforts should be devoted to investigating the role of connections between the building and the exoskeletons, and the effect of the soil–structure interaction in the ISD threshold evaluation of RC moment-resisting frames retrofitted with exoskeletons.

CRediT authorship contribution statement

Raffaele Cucuzza: Writing – review & editing, Writing – original draft, Validation, Methodology, Investigation, Formal analysis, Conceptualization. **Jana Olivo:** Writing – review & editing, Writing – original draft, Visualization, Validation, Software, Methodology, Investigation, Formal analysis, Data curation. **Gabriele Bertagnoli:** Writing – review & editing, Validation, Supervision, Methodology, Investigation. **Giuseppe Andrea Ferro:** Writing – review & editing, Supervision, Funding acquisition, Conceptualization. **Giuseppe Carlo Marano:** Supervision, Methodology, Funding acquisition, Conceptualization.

Declaration of competing interest

The authors declare that they have no known competing financial interests or personal relationships that could have appeared to influence the work reported in this paper.

Acknowledgments

The research leading to these results has received funding from the European Research Council under the Grant agreement ID: 101007595 of the project ADDOPTML, MSCA RISE 2020 Marie Skodowska Curie Research and Innovation Staff Exchange (RISE). This study was partially developed within the research activities carried out in the framework of the 2022–2024 ReLUIS Project—WP5.1 (Coordinators — G.A. Ferro, R. Cucuzza)

Appendix

In this Appendix, the cross-sections and reinforcement of the Reinforced Concrete elements constituting the existing buildings are provided in Table A.5. In Table A.6, the cross-sections of the standard Circular Hollow Sections (CHS) that constitute the exoskeletons, selected by the optimization process, are presented. These sections correspond to the design for the inter-story drift (ISD) thresholds of H/650, which is the most restrictive and steel-demanding case.

Table A.6
CHS profiles of the exoskeleton's elements (DVs in Fig. 5) selected through the optimization process for each Case Study (CS#), with an inter-story drift threshold of H/650. Diameter (⌀) and thickness (t) are expressed in mm.

		x_1	x_2	x_3	x_4	x_5	x_6	x_7	x_8	x_9
CS1	⌀	457	355.6	323.9	508	406.4	177.8	219.1	323.9	323.9
	t	40	25	20	30	30	10	10	14.2	25
CS2	⌀	711	406.4	355.6	711	406.4	219.1	219.1	406.4	323.9
	t	30	30	20	30	30	10	10	14.2	25
CS3	⌀	508	457	406.4	762	508	219.1	244.5	323.9	406.4
	t	50	40	30	30	30	10	14.2	20	30

Data availability

No data was used for the research described in the article.

References

[1] A.A. Kelam, S. Karimzadeh, K. Yousefibavil, H. Akgün, A. Askan, M.A. Erberik, M.K. Koçkar, O. Pekcan, H. Ciftci, An evaluation of seismic hazard and potential damage in Gaziantep, Turkey using site specific models for sources, velocity structure and building stock, Soil Dyn. Earthq. Eng. 154 (2022) 107129.

[2] P. Foraboschi, Versatility of steel in correcting construction deficiencies and in seismic retrofitting of RC buildings, J. Build. Eng. 8 (2016) 107–122.

[3] H. Crowley, J. Dabbeek, V. Despotaki, D. Rodrigues, L. Martins, V. Silva, X. Romão, N. Pereira, G. Weatherill, L. Danciu, European seismic risk model (ESRM20), EFEHR Tech. Rep. 2 (2021).

[4] C. Corbane, U. Hancilar, D. Ehrlich, T. De Groeve, Pan-European seismic risk assessment: a proof of concept using the earthquake loss estimation routine (ELER), Bull. Earthq. Eng. 15 (2017) 1057–1083.

[5] Building Performance Institute Europe (BPIE), Europe's Buildings Under the Microscope: A Country-By-Country Review of the Energy Performance of the Buildings, Brussels, 2011.

[6] A. Reggio, L. Restuccia, L. Martelli, G.A. Ferro, Seismic performance of exoskeleton structures, Eng. Struct. (ISSN: 0141-0296) 198 (2019) 109459, http://dx.doi.org/10.1016/j.engstruct.2019.109459.

[7] G. Di Lorenzo, E. Colacurcio, A. Di Filippo, A. Formisano, A. Massimilla, R. Landolfo, State-of-the-art on steel exoskeletons for seismic retrofit of existing RC buildings, Int. J. 37 (1–2020) (2020).

[8] M. Domaneschi, R. Cucuzza, Structural resilience through structural health monitoring: A critical review, Data Driven Methods Civ. Struct. Heal. Monit. Resil. (2024) 1–13.

[9] M. Domaneschi, R. Cucuzza, L. Martinelli, M. Noori, G.C. Marano, A probabilistic framework for the resilience assessment of transport infrastructure systems via structural health monitoring and control based on a cost function approach, Struct. Infrastruct. Eng. (2024) 1–13.

[10] C. Passoni, A. Marini, A. Belleri, C. Menna, A multi-step design framework based on life cycle thinking for the holistic renovation of the existing buildings stock, in: IOP Conference Series: Earth and Environmental Science, Vol. 290, IOP Publishing, 2019, 012134.

[11] A. Caverzan, M. Lamperti Tornaghi, P. Negro, Roadmap for the improvement of earthquake resistance and eco-efficiency of existing buildings and cities, in: Proceedings of SAFESUST Workshop; JRC, JRC Science Hub: Ispra, Italy, 2015, pp. 1–136.

[12] A.S. of Civil Engineers, Minimum Design Loads for Buildings and Other Structures, American Society of Civil Engineers, 2013.

[13] G. Di Lorenzo, A. Prota, Orthogonal steel exoskeleton for low impact and rapid execution retrofitting of existing buildings: State-of-the-art and structural concept, in: AIP Conference Proceedings, Vol. 3094, AIP Publishing, 2024.

[14] A. Reggio, R. Greco, G.C. Marano, G.A. Ferro, Stochastic multi-objective optimisation of exoskeleton structures, J. Optim. Theory Appl. 187 (2020) 822–841.

[15] R. Cucuzza, A. Aloisio, M. Domaneschi, R. Nascimbene, Multimodal seismic assessment of infrastructures retrofitted with exoskeletons: Insights from the foggia airport case study, Bullettin Earthq. Eng. (2024).

[16] A. Prota, R. Tartaglia, G. Di Lorenzo, R. Landolfo, Seismic strengthening of isolated RC framed structures through orthogonal steel exoskeleton: Bidirectional non-linear analyses, Eng. Struct. 302 (2024) 117496.

[17] G. Di Lorenzo, R. Tartaglia, A. Prota, R. Landolfo, Design procedure for orthogonal steel exoskeleton structures for seismic strengthening, Eng. Struct. 275 (2023) 115252.

[18] E. Meglio, A. Formisano, Design and modelling strategy for cold-formed steel exoskeletons for the seismic-energy retrofit of reinforced concrete structures, in: Structures, Vol. 69, Elsevier, 2024, 107502.

[19] E. Meglio, A. Formisano, Seismic design and analysis of a cold-formed steel exoskeleton for the retrofit of an RC multi-story residential building, Appl. Sci. 14 (19) (2024) 8674.

[20] F. Mazza, Dissipative steel exoskeletons for the seismic control of reinforced concrete framed buildings, Struct. Control. Heal. Monit. 28 (3) (2021) e2683.

[21] M. Domaneschi, Simulation of controlled hysteresis by the semi-active bouc-wen model, Comput. Struct. 106 (2012) 245–257.

[22] R. Cucuzza, M. Domaneschi, R. Greco, G.C. Marano, Numerical models comparison for fluid-viscous dampers: Performance investigations through genetic algorithm, Comput. Struct. 288 (2023) 107122.

[23] R. Cucuzza, M. Domaneschi, M.M. Rosso, L. Martinelli, G.C. Marano, Cutting stock problem (CSP) applied to structural optimization for the minimum waste cost, Ce/ Pap. 6 (5) (2023) 1066–1073.

[24] R. Cucuzza, M.M. Rad, M. Domaneschi, G.C. Marano, Sustainable and cost-effective optimal design of steel structures by minimizing cutting trim losses, Autom. Constr. 167 (2024) 105724.

[25] A. Belleri, A. Marini, Does seismic risk affect the environmental impact of existing buildings? Energy Build. 110 (2016) 149–158.

[26] E. Frangedaki, L. Sardone, N.D. Lagaros, Design optimization of tree-shaped structural systems and sustainable architecture using bamboo and earthen materials, J. Archit. Eng. 27 (4) (2021).

[27] C. Passoni, J. Guo, C. Christopoulos, A. Marini, P. Riva, Design of dissipative and elastic high-strength exoskeleton solutions for sustainable seismic upgrades of existing RC buildings, Eng. Struct. 221 (2020) 111057.

[28] A. Marini, C. Passoni, A. Belleri, F. Feroldi, M. Preti, G. Metelli, P. Riva, E. Giuriani, G. Plizzari, Combining seismic retrofit with energy refurbishment for the sustainable renovation of RC buildings: A proof of concept, Eur. J. Environ. Civ. Eng. 26 (7) (2022) 2475–2495.

[29] E. Meglio, G. Longobardi, A. Formisano, Integrated seismic-energy retrofit systems for preventing failure of a historical RC school building: Comparison among metal lightweight exoskeleton solutions, Eng. Fail. Anal. 154 (2023) 107663.
[30] R. Tartaglia, A. Prota, A. Milone, G. Di Lorenzo, R. Landolfo, Seismic assessment and strengthening of an existing industrial building, in: International Conference on the Behaviour of Steel Structures in Seismic Areas, Springer, 2022, pp. 966–974.
[31] F. Feroldi, A. Marini, A. Belleri, C. Passoni, P. Riva, M. Preti, E. Giuriani, G. Plizzari, Miglioramento e adeguamento sismico di edifici contemporanei mediante approccio integrato energetico, architettonico e strutturale con soluzioni a doppio involucro a minimo impatto ambientale, Progett. Sismica. Ital. (2) (2014).
[32] A. Marini, C. Passoni, P. Riva, P. Negro, E. Romano, F. Taucer, et al., Technology options for earthquake resistant, eco-efficient buildings in europe: Research needs, Eur. Comm. Jt. Res. Cent. Sci. Policy Rep. (2014).
[33] A. Prota, R. Tartaglia, R. Landolfo, Improving seismic performance of existing schools: Design and analysis of steel exoskeleton systems, in: International Conference on the Behaviour of Steel Structures in Seismic Areas, Springer, 2024, pp. 564–575.
[34] U. Saracco, E. Meglio, A. Formisano, Seismic-energy combined retrofit systems of historical buildings: The use of light metal exoskeletons, Tech. Ann. 1 (3) (2023).
[35] M. De Vita, S. Panunzi, G. Fabbrocino, A. Mannella, A discussion on the conceptual design of multifunctional exoskeletons for sustainable regeneration of buildings in urban areas, Buildings 12 (8) (2022) 1100.
[36] A. Marini, A. Belleri, C. Passoni, F. Feroldi, M. Preti, G. Metelli, E. Giuriani, P. Riva, G. Plizzari, Integrated architectural, energy and seismic renovation of the reinforced concrete building stock targeting sustainability and resilience, Submitt. J. Civ. Environ. Eng. (2016).
[37] A. Caverzan, M. Lamperti Tornaghi, P. Negro, Taxonomy of the redevelopment methods for non-listed architecture: from façade refurbishment to the exoskeleton system, in: JRC, Conference and Workshop Reports, Proceedings of Safesust Workshop, Ispra, November, 2016, pp. 26–27.
[38] S. D'Urso, B. Cicero, From the efficiency of nature to parametric design. a holistic approach for sustainable building renovation in seismic regions, Sustain. 11 (5) (2019) 1227.
[39] A. Marini, A. Belleri, F. Feroldi, C. Passoni, M. Preti, P. Riva, E. Giuriani, G. Plizzari, Coupling energy refurbishment with structural strengthening in retrofit interventions, in: SAFESUST Workshop, SAFESUST Ispra, Italy, 2015, pp. 26–27.
[40] C. Passoni, Holistic Renovation of Existing RC Buildings: a Framework for Possible Integrated Structural Interventions (Ph.D. thesis), Ph. D. thesis, University of Brescia, 2016.
[41] L. Martelli, L. Restuccia, G. Ferro, The exoskeleton: a solution for seismic retrofitting of existing buildings, Procedia Struct. Integr. 25 (2020) 294–304.
[42] European Committee for Standardization (CEN), Design of Structures for Earthquake Resistance, Brussels, Belgium, 2005.
[43] S. Labò, C. Passoni, A. Marini, A. Belleri, Design of diagrid exoskeletons for the retrofit of existing rc buildings, Eng. Struct. 220 (2020) 110899.
[44] G.C. Marano, G. Quaranta, Robust optimum criteria for tuned mass dampers in fuzzy environments, Appl. Soft Comput. J. 9 (4) (2009) 1232–1243.
[45] A. Reggio, L. Restuccia, L. Martelli, G.A. Ferro, Seismic performance of exoskeleton structures, Eng. Struct. 198 (2019) 109459.
[46] V. Ciampi, M. De Angelis, F. Paolacci, Design of yielding or friction-based dissipative bracings for seismic protection of buildings, Eng. Struct. 17 (5) (1995) 381–391.
[47] D. D'Agostino, D. Faiella, E. Febbraro, E. Mele, F. Minichiello, J. Trimarco, Steel exoskeletons for integrated seismic/energy retrofit of existing buildings-general framework and case study, J. Build. Eng. 83 (2024) 108413.
[48] DM17/01/2018, Aggiornamento delle "Norme tecniche per le costruzioni", Italian Ministry of Infrastructures and Transportation, Rome, Italy, 2018, in Italian.
[49] EN1998-1, Eurocode 8: Eurocode 8: Design of structures for earthquake resistance – Part 1: General rules, seismic actions and rules for buildings, The European Union Per Regulation, Brussels, Belgium, 2004.
[50] S.E. Institute, ASCE Standard, ASCE/SEI, 41-17, Seismic Evaluation and Retrofit of Existing Buildings, American Society of Civil Engineers, Reston, Virginia, 2017.
[51] F. Kazemi, N. Asgarkhani, R. Jankowski, Machine learning-based seismic response and performance assessment of reinforced concrete buildings, Arch. Civ. Mech. Eng. 23 (2) (2023) 94.
[52] F. Kazemi, N. Asgarkhani, R. Jankowski, Machine learning-based seismic fragility and seismic vulnerability assessment of reinforced concrete structures, Soil Dyn. Earthq. Eng. 166 (2023) 107761.
[53] N. Asgarkhani, F. Kazemi, R. Jankowski, Machine learning-based prediction of residual drift and seismic risk assessment of steel moment-resisting frames considering soil-structure interaction, Comput. Struct. 289 (2023) 107181.
[54] G.C. Marano, G. Quaranta, R. Greco, Multi-objective optimization by genetic algorithm of structural systems subject to random vibrations, Struct. Multidiscip. Optim. 39 (4) (2009) 385–399.
[55] J. Olivo, R. Cucuzza, G. Bertagnoli, M. Domaneschi, Optimal design of steel exoskeleton for the retrofitting of rc buildings via genetic algorithm, Comput. Struct. 299 (2024) 107396.
[56] A. Ghobarah, On drift limits associated with different damage levels, in: International Workshop on Performance-Based Seismic Design, Vol. 28, Department of Civil Engineering, McMaster University Ontario, Canada, 2004.
[57] Y. Lu, X. Gu, J. Guan, Probabilistic drift limits and performance evaluation of reinforced concrete columns, J. Struct. Eng. 131 (6) (2005) 966–978.
[58] A.S. of Civil Engineers (ASCE), FEMA 356: Prestandard and Commentary for the Seismic Rehabilitation of Buildings, Federal Emergency Management Agency (FEMA), Washington, D.C., 2000.
[59] EN1993-1-1, Eurocode 3: Design of Steel Structures - Part 1-1: General Rules and Rules for Buildings, The European Union Per Regulation, Brussels, Belgium, 2005.